

# Interplay of Quasi-Quantum Hall Effect and Coulomb Disorder in Semimetals

Ian A. Leahy,<sup>1</sup> Anthony D. Rice,<sup>1</sup> Jocienne N. Nelson,<sup>1,\*</sup> Herve Ness,<sup>2</sup> Mark van Schilfgaarde,<sup>1</sup> Wei Pan,<sup>3</sup> and Kirstin Alberi<sup>1,4,†</sup>

<sup>1</sup>*National Renewable Energy Laboratory, Golden, Colorado 80401, USA*

<sup>2</sup>*Department of Physics, King's College London, Strand, London WC2R 2LS, United Kingdom*

<sup>3</sup>*Materials Physics Department, Sandia National Laboratories, Livermore, California 94551, USA*

<sup>4</sup>*Renewable and Sustainable Energy Institute, National Renewable Energy Laboratory and University of Colorado, Boulder, 80301, CO, United States*

Low carrier densities in topological semimetals (TSMs) enable the exploration of novel magneto-transport in the quantum limit (QL). Reports consistent with 3D quasi-quantum Hall effect (QQHE) have repositioned TSMs as promising platforms for exploring 3D quantum Hall transport, but the lack of tunability in the Fermi has thus far limited the ability to control the QQHE signal. Here, we tune the defect concentrations in the Dirac semimetal Cd<sub>3</sub>As<sub>2</sub> to achieve ultra-low carrier concentrations at 2 K around  $2.9 \times 10^{16} \text{cm}^{-3}$ , giving way to QQHE signal at modest fields under 10 T. At low carrier densities, where QQHE is most accessible, we find that a zero resistivity state is obscured by a carrier density dependent background originating from Coulomb disorder from charged point defects. Our results highlight the interplay between QQHE and Coulomb disorder scattering, demonstrating that clear observation of QQHE in TSMs intricately depends on Fermi level. Predicted in TSMs a decade ago, we find that Coulomb disorder is an essential ingredient for understanding the magnetoresistivity for a spectrum of Fermi levels, experimentally anchoring the important roles of defects and charged disorder in TSM applications. We discuss future constraints and opportunities in exploring 3D QHE in TSMs.

**Keywords:** Quasi Quantum Hall Effect, Coulomb Disorder, Topological Semimetals

The 2D quantum Hall effect (QHE) is a hallmark of two-dimensional electron systems in magnetic fields, resulting in the integer quantized plateaus of the Hall resistivity  $\rho_{xy}$  paired with vanishingly small longitudinal resistivity,  $\rho_{xx}$  [1, 2]. This quantized effect, observable across a spectrum of material systems regardless of chemical composition or disorder, is accompanied by dissipationless chiral edge states [3, 4]. The 2D QHE has sparked decades of research on related effects, enabled high fidelity measurements of fundamental constants ( $h/e^2$ ), generated many potential applications in spintronics and quantum computing [5, 6], and critically, has helped elucidate the role of topology in the study of electronic band structures. Understanding the 3D analog, the quasi-quantum Hall effect (QQHE), stands to make a similar impact – unveiling new quantum Hall (QH) states of matter with accompanying 2D surface states. Topological semimetals (TSMs) are promising candidates for hosting the QQHE as high mobilities ensure  $\rho_{xy} \approx \sigma_{xy}^{-1}$  (where  $\sigma_{xy}$  is the Hall conductivity) and low carrier densities enable visible QH features at accessible fields [7, 8]. As the presence of disorder is necessary for the 2D QHE and electron-electron interactions are required for realizing fractional QHE, low Fermi energies combined with Coulomb disorder in TSMs may produce a promising route for realizing 3D fractionalized QQHE analogues. To explore this new physics, we must first understand the QQHE magnetotransport in systems complicated by magnetic-field-dependent Coulomb disorder scattering.

Mechanisms for the 3D QQHE are similar to the 2D

QHE but with additional dispersion along the applied field direction [7, 8, 10]. In 2D, the quantized Hall conductivity arises from the interplay of dimensionality, Landau bands (LBs), and disorder. An applied magnetic field changes the free carrier Hamiltonian to that of a shifted harmonic oscillator, defining the highly degenerate LBs and discretizing the density of states (DOS) into delta functions. Increasing the applied magnetic field, LBs moving through the Fermi level offer finite then vanishing DOS, yielding quantized jumps in the Hall conductivity. Disorder is a central ingredient in the observation of the 2D QHE. Charged point defects broaden the LB  $\delta$ -DOS, responsible for the finite field extent of the rise between plateaus. The quantum Hall plateau indicates that the number of filled LB in a system has not changed, enabled by the localization of a portion of charge carriers around disorder sites [11, 12].

Though predicted, experimental realizations of the 3D QHE have remained elusive. In particular, many observations reduce to weakly coupled stacks of 2D QHE systems. Recently, low carrier density metallic and TSM systems have renewed the search for 3D quantum Hall states [7, 8, 10, 13–16]. As in 2D, signatures of the 3D QHE state should also involve vanishing  $\rho_{xx}$  and quantized, step-like  $\rho_{xy}$ , though no experimental confirmations of this perfect quantization have been observed. Efforts in the weakly gapped 3D Dirac semimetals ZrTe<sub>5</sub> and HfTe<sub>5</sub> have revealed that  $\rho_{xy}$  is quasi-quantized.  $\rho_{xx}$  is always finite, yet exhibits well defined maxima/minima that are correlated to flatter – but not constant – regions in  $\rho_{xy}$  (Fig. 1b). As magnetotransport holds the key to identifying and characterizing QQHE, understanding the mechanisms yielding finite  $\rho_{xx}$  and preventing the true

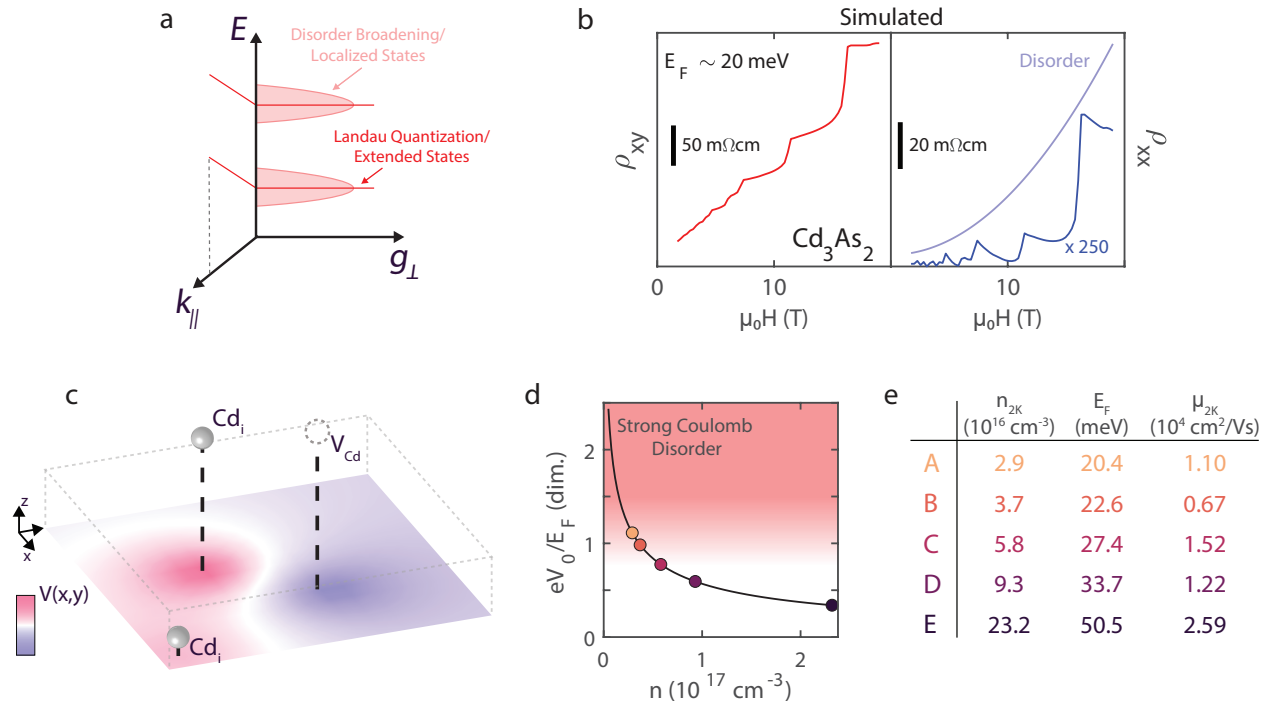


FIG. 1. **3D QQHE and Coulomb disorder in 3D TSMs** a) Schematic density of states for a 3D QQHE system under an applied field. As in 2D, disorder serves to broaden the Dirac-delta-function like DOS (perpendicular to the field), introducing a range of localized states. Additionally in 3D, carriers maintain dispersion along the applied field direction. b) Calculated  $\rho_{xy}$  (red, left) and  $\rho_{xx}$  (blue, right) using a k.p model for  $\text{Cd}_3\text{As}_2$  with  $E_F = 20$  meV. Clear plateau-like features emerge in  $\rho_{xy}$  and correlate to bump like features in  $\rho_{xx}$ . The presence of disorder will tend to smear these features and introduce additional smooth magnetic field dependence. The light blue trace represents a magnetoresistance possible in the presence of disorder (Methods and Supplementary Note 1). c) Cd interstitials and vacancies are critical to understanding the magnetotransport of  $\text{Cd}_3\text{As}_2$ . These disorder types are energetically favorable, charged, and dense, reaching  $\sim 10^{18}$  cm $^{-3}$  in some  $\text{Cd}_3\text{As}_2$  thin films. The charged disorder sites, paired with screening, generate a disorder potential responsible for linear MR in high  $E_F$  films. The colorplot shows a slice of the potential,  $V(x,y)$ , at the plane defined by the dashed line. d) Ratio of the average disorder potential strength to the Fermi level as a function of  $n$ , calculated using Ref. [9] and relevant values for  $\text{Cd}_3\text{As}_2$  (see SI Section 1). Colored circles represent Samples A-E presented here. As the carrier density decreases,  $\text{Cd}_3\text{As}_2$  moves into the strong Coulomb disorder limit. e) Table summarizing carrier densities, Fermi levels, and mobilities for Samples A-E. Carrier densities extracted from the low field slope of  $\rho_{xy}(H)$  are used in combination with the DOS to estimate  $E_F$  (See Supplementary Note 1).

3D QHE state are of paramount importance.

$\text{Cd}_3\text{As}_2$  is a compelling candidate for exploring the interplay of the 3D QQHE and Coulomb disorder, shedding light onto the mechanisms diluting the vanishing  $\rho_{xx}$ . Additionally, as a gapless TSM,  $\text{Cd}_3\text{As}_2$  opens the possibility to explore exotic states emerging from interactions between QHE surface states and gapless TSM bulk. In the 3D QQHE, Coulomb disorder likely serves a similar role in localization and the broadening of LBs. In addition, Coulomb disorder has been predicted and shown to have serious implications on the magnetotransport of TSMs [9, 17]. We have previously shown weak Coulomb disorder to be central in explaining the linear, non-saturating magnetoresistance in TSMs. The Fermi level (defined relative to the Dirac point),  $E_F$ , in  $\text{Cd}_3\text{As}_2$  is set by the defect concentrations of charged cadmium

vacancies and interstitials [18, 19]. These charged defect sites become screened, contingent on the carrier density, resulting in a disorder potential (Fig. 1c). In  $\text{Cd}_3\text{As}_2$ , linear MR has been used to determine disorder potential energies,  $eV_0 \sim 15 - 25$  meV consistent with theoretical predictions and STM experiments on similar materials [9, 17, 20, 21]. These measurements were performed in the weak Coulomb disorder limit, when  $eV_0 < E_F$ . Tuning the Fermi level lower simultaneously increases the average disorder potential because of reduced screening, leading to an increase in  $eV_0/E_F$  as shown in Fig. 1d for  $\text{Cd}_3\text{As}_2$ . Lowering the carrier density in  $\text{Cd}_3\text{As}_2$  will concurrently affect two phenomena with magnetotransport implications: the QQHE and a transition from weak to strong Coulomb disorder. Explicitly, decreasing  $n$  shrinks the field scale of the quantum limit (QL) making

the QQHE easier to experimentally resolve. At the same time, transitioning from the weak to strong Coulomb disorder limit will alter the magnetotransport and cause charge puddling and local rigid band shifts smearing  $E_F$ . The inclusion of disorder serves to broaden out the QQHE and introduce a non-QQHE background (Fig. 1b, Methods, and Supplementary Note 1). Thus,  $\text{Cd}_3\text{As}_2$  provides an opportunity to explore a gapless QQHE material with tunable Coulomb disorder – a model system for investigating the 3D QHE.

In this paper, we study the electrical transport in low carrier density, (001)- $\text{Cd}_3\text{As}_2$  bulk-like thin films. We find the low carrier density magnetotransport to be described as a superposition of the QQHE and Coulomb disorder scattering. MBE growth allows the tuning of the carrier density in the range of  $\sim 2 - 20 \times 10^{16} \text{ cm}^{-3}$  (Fig. 1e) unlocking a range of Coulomb disorder strengths and shifting the QQHE field scales, yielding a measurement of the interplay between these effects. The benefits of MBE growth over bulk semimetals are twofold, extending Fermi level control beyond what is possible in bulk and offering a QQHE platform with a realistic avenue for disorder control. Our observations serve to confirm the existence of QQHE in a 3D gapless Dirac semimetal as well as help to understand the role of Coulomb disorder in TSM magnetotransport, generating actionable insight into the exploration and enhancement of 3D QHE in many semimetal systems. Coulomb disorder contributes strongly to the longitudinal resistivity and is a likely contributor to non-vanishing  $\rho_{xx}$  across QQHE materials. We conclude with a discussion of routes for further investigation of the QQHE in  $\text{Cd}_3\text{As}_2$ .

## RESULTS

We begin by exploring the 2 K magnetotransport in two  $\text{Cd}_3\text{As}_2$  films with differing carrier densities. Fig. 2a-c are obtained on Sample E, a high carrier density film with  $n_{2\text{K}} = 2.3 \times 10^{17} \text{ cm}^{-3}$  (Fig. 1e). The fractional magnetoresistance (FMR =  $[\rho_{xx}(H) - \rho_0]/\rho_0 \times 100\%$ , where  $\rho_0 \equiv \rho_{xx}(0\text{T})$ ) scales linearly with increasing field with superimposed quantum oscillations (Fig. 2a). The Hall resistivity,  $\rho_{xy}$ , is linear with visible quantum oscillations, consistent with a single, electron-like carrier (Fig. 2b). Lastly, the tangent of the Hall angle,  $\tan \theta_H \equiv \rho_{xy}/\rho_{xx}$ , rapidly increases at low fields and saturates to a constant, field-independent value, less any quantum oscillations (Fig. 2c). This behavior is standard and has been observed in many TSMs [19, 22].

We now turn to Sample C, shown in Fig. 2d-f, having  $n_{2\text{K}} = 5.8 \times 10^{16} \text{ cm}^{-3}$ . The 2 K FMR (Fig. 2d) shows quadratic growth near zero field, followed by a shoulder near 3.5 T, defined as  $H_S$ , above which the FMR continues to increase rapidly and non-linearly. Remnants of this structure are visible in data up to 80 K. Correspondingly,

$\rho_{xy}$  exhibits a peculiar and distinct change in slope at  $H_S$  which also remains visible to higher temperatures (Fig. 2e). Finally,  $\tan \theta_H$  shares the usual low-field increase, but does not saturate as in the high-density sample, exhibiting a large lump near 5 T reflecting the structure of the underlying resistivities.

The change in slope of the Hall resistivity near  $H_S$  is striking and is distinct from a typical quantum oscillation. Potential origins of this magnetotransport are: i) multiband transport, ii) Berry curvature induced effects, iii) localization, iv) disorder scattering, and v) QQHE. A two band model can generate non-linear Hall effect and quadratic magnetoresistance, but multiple (or anisotropic) bands are necessary to generate a magnetoresistance with a rapidly changing magnetic field dependence. Likewise, nonmonotonicity in the Hall effect of multiband models is typically smooth as a function of field, contrasting with the sharp slope change observed here. With a single band crossing the Fermi level, a multiband picture is difficult to justify. In the study of some TSMs, particular Weyl semimetals, sharp slope changes in  $\rho_{xy}$  have been correlated with anomalous-like Hall effects originating from non-trivial, divergenceful, Berry curvature originating from k-space-separated Weyl points. In  $\text{Cd}_3\text{As}_2$  the four-fold degenerate Dirac point splits into two sets of Weyl points along an applied field direction but those sets of Weyl points are of opposite chirality, minimizing Berry-curvature effects. Finally, weak localization effects should be minimal. Weak antilocalization, a quantum interference effect leading to a positive magnetoresistance, has been observed in thin films ( $< 100 \text{ nm}$ ) of  $\text{Cd}_3\text{As}_2$ . Observation of localization effects is typically limited to low temperatures [26–28]. Further, magnetic fields destroy the requisite coherence necessary for the effects, restricting observation of the localization magnetoresistance to much less than 1 T. The magnitude of the effects shown in Fig. 2d-f, the extent of the effects in field, and the simultaneous features in the FMR and  $\rho_{xy}$  rule out localization.

For high carrier density  $\text{Cd}_3\text{As}_2$ , disorder is a crucial ingredient in determining the magnetotransport. Scattering from the disorder potential landscape, generated from screened Coulomb disorder, yields linear MR. The FMR in Sample E is dominated by this scattering as the high field MR is linear and  $\tan \theta_H$  saturates to a constant value [19]. For lower carrier density  $\text{Cd}_3\text{As}_2$ , the reduced  $\Delta E \equiv E_F - E_{DP}$  and consequent reduced charged defect screening results in a larger average disorder potential. The Coulomb disorder which yields linear MR in the high carrier density, weak disorder strength limit becomes stronger in lower density samples. The linear magnetic field dependence of the magnetoresistance can change as the Coulomb disorder becomes stronger [29]. Altogether, the super-quadratic high field MR is likely indicative of the weak-to-strong crossover of the Coulomb disorder while the non-monotonicity of the FMR indi-

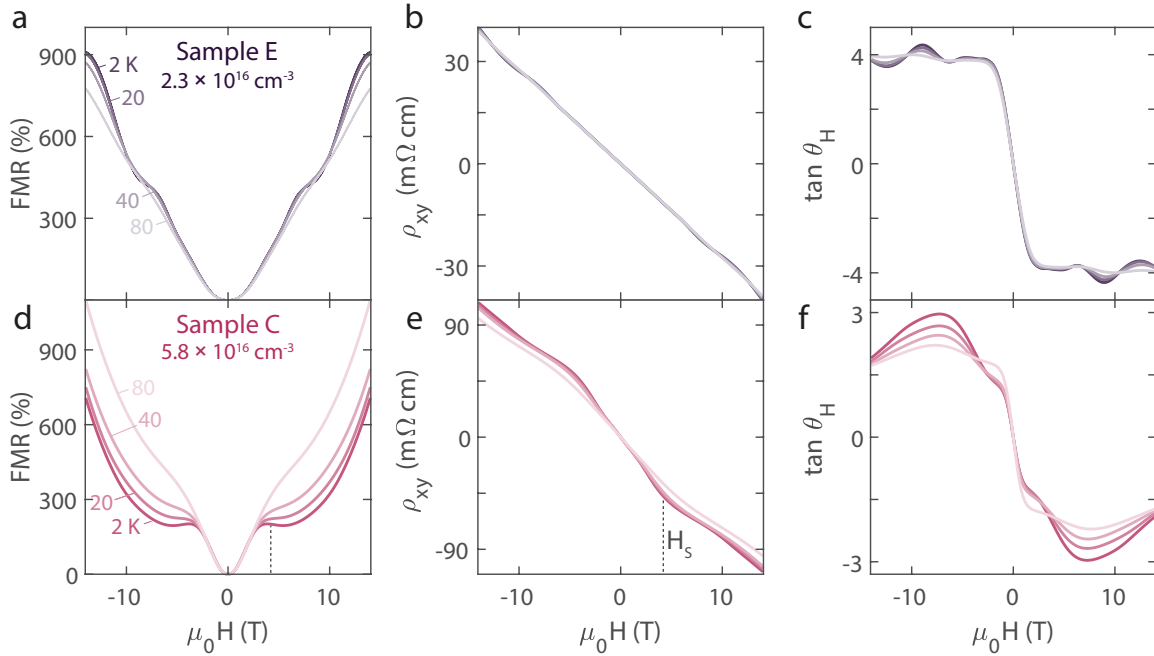


FIG. 2. **Carrier density tunes magnetotransport in  $\text{Cd}_3\text{As}_2$ .** a,d) Fractional magnetoresistance, b,e) Hall resistivity, and c,f) tangent of the Hall angle  $\tan \theta_H \equiv \rho_{xy}/\rho_{xx}$  at several temperatures for a  $\text{Cd}_3\text{As}_2$  films with low temperature electron carrier densities of (a-c) Sample E:  $2.3 \times 10^{17} \text{ cm}^{-3}$  and (d-f) Sample C:  $5.8 \times 10^{16} \text{ cm}^{-3}$ . Sample E shows linear MR and Hall effect with superimposed quantum oscillations. Meanwhile,  $\tan \theta_H$  saturates to a constant value. On the other hand, Sample C shows a low field quadratic and high field super-quadratic MR and a clear kink in  $\rho_{xy}$ .

cates that Coulomb disorder scattering is only part of the picture.

Recently, strikingly similar magnetotransport to that of Sample C has been observed in the zirconium and hafnium pentatellurides [7, 10, 15, 16]. Investigations in  $\text{ZrTe}_5$  culminated in the discovery of a three-dimensional QHE, the so-called quasi-quantum Hall effect. Much like the 2D QHE, the QQHE exhibits lumps in  $\rho_{xx}$  paired with plateau-like features in  $\rho_{xy}$ . Correspondingly,  $\tan \theta_H$  will approach some large value with periodic decreases between Hall plateaus. The 3D dispersion and other material parameters make it difficult to observe strictly vanishing  $\rho_{xx}$  and exact  $\rho_{xy}$  plateaus. Generically, the observation of clean  $\rho_{xy}$  plateaus and  $\rho_{xx}$  bumps in 3D metallic or semimetallic systems relies upon both low carrier concentrations and sizeable mobilities. In  $\text{ZrTe}_5$  and  $\text{HfTe}_5$ , low carrier densities ( $0.9\text{-}2 \times 10^{17} \text{ cm}^{-3}$ ) paired with high mobilities are naturally accompanied by a  $\tan \theta_H \sim 10$  in the QL. Low carrier concentrations ensure that QL-sized fields can be attained with experimental ease (1-2 T) and high mobilities ( $2\text{-}50 \times 10^4 \text{ cm}^2/\text{Vs}$ ) yield clearer QQHE features by ensuring  $\rho_{xy} \sim \sigma_{xy}^{-1}$  [7, 10]. In the 2D QHE, the longitudinal and Hall resistivities are related such that  $\rho_{xx} = -\alpha H \partial_H \rho_{xy}$ . A similar scaling is expected to hold in the 3D QQHE [8].

In contrast to the cases of the pentatellurides, we

observe far fewer quantum oscillations in our  $\text{Cd}_3\text{As}_2$ , though magnetotransport at different fixed magnetic field angles are consistent with a 3D Fermi surface. The low carrier density and requisite small Fermi surface size implies a low frequency of oscillation in  $\text{Cd}_3\text{As}_2$ . Additionally, the mobilities in our films limit where quantum oscillations are visible. Finally, the screening of charged point defects are accompanied by local rigid band shifts, serving to further broaden LBs. The step-like  $\rho_{xy}$  measured in Sample C is consistent with a weak QQHE signal superimposed with a conventional Hall resistivity. The relatively weaker plateaus in  $\text{Cd}_3\text{As}_2$  are likely the result of significant LB broadening, low mobilities spoiling the direct inversion  $\rho_{xy} = \sigma_{xy}^{-1}$ , Coulomb disorder scattering leading to large  $\rho_{xx}$ , and the screening of Coulomb disorder smearing  $E_F$  throughout the sample. Overall, we hypothesize that the magnetotransport is a superposition of QH and Coulomb disorder scattering effects.

We turn our attention to the magnetotransport for additional samples with varying carrier densities. Varying the carrier density will simultaneously alter the field scales of the observed QQHE as well as change the effective Coulomb disorder strength through the screening of defects. Figure 3 show  $\rho_{xx}$  (a-d) as dark colored lines for  $\mu_0 H < 0$  T and  $\rho_{xy}$  (e-h). Sample carrier densities increase from top to bottom. As expected with decreasing carrier density, the slope of the Hall effect and the

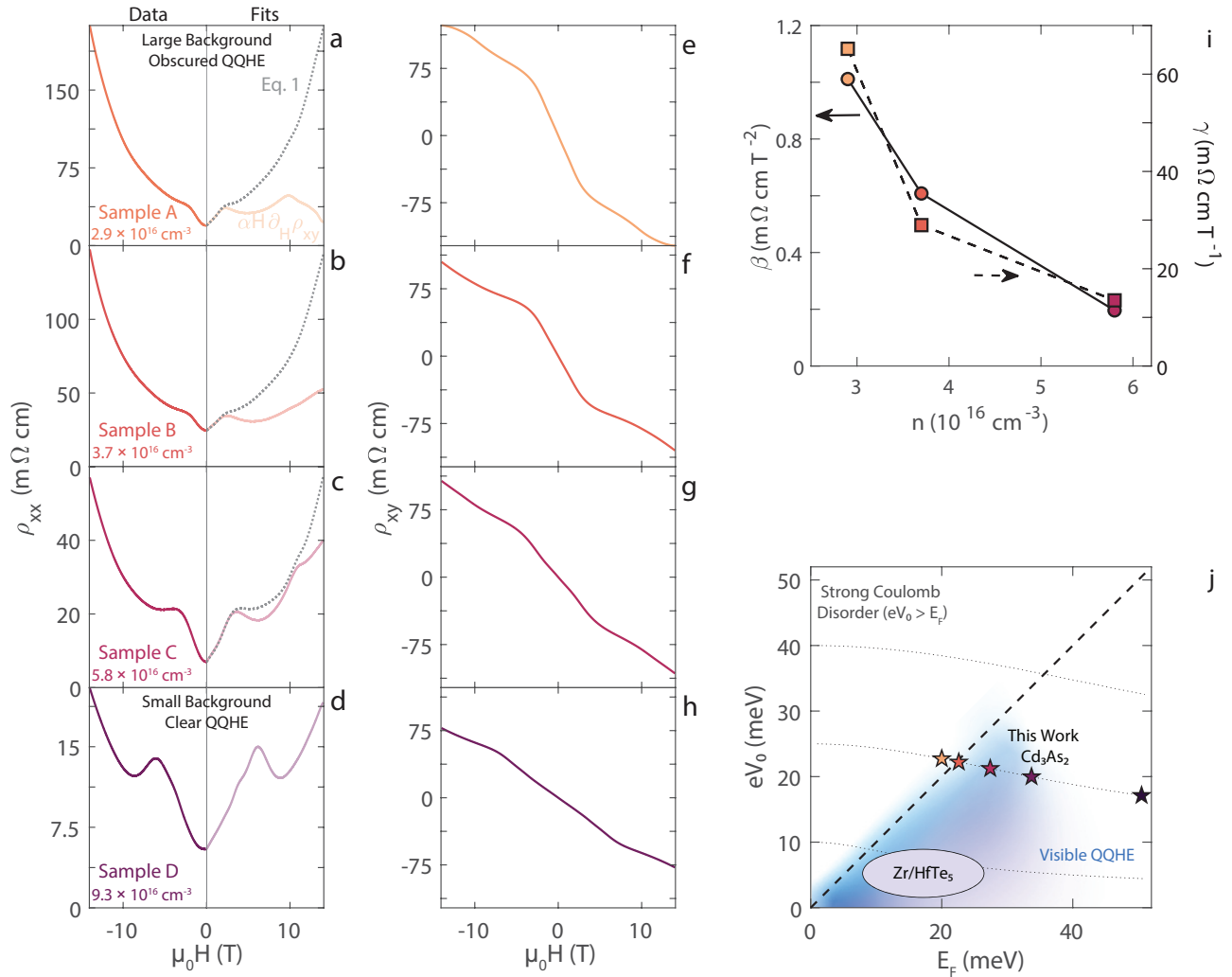


FIG. 3. **QQHE and Coulomb scattering in Cd $_3$ As $_2$ .** a-d) Longitudinal and e-h) Hall resistivity for samples of increasing carrier density at 5 K. In panels a-d, the left half of the axes correspond to raw data while the right half show fits of the data to only the QQHE (light color, solid) and to the full Eq. 1 (gray, dotted). Eq. 1 was not fit to Sample D as it lies in the weak Coulomb disorder limit. i) Carrier density dependence of  $\beta$  and  $\gamma$  fit parameters from Eq. 1. j) A plot of the disorder potential strength calculation vs. the Fermi level for Cd $_3$ As $_2$ . Significant Coulomb disorder in Cd $_3$ As $_2$  combats a clean observation of the QQHE. Meanwhile, for ZrTe $_5$  and HfTe $_5$ , stronger screening of charged disorder means weaker contributions from Coulomb disorder scattering. Estimates for the pentatelluride systems from [7, 10, 15, 16, 23–25]. Dotted lines represent calculated contours of how  $eV_0$  changes with Fermi level from Ref. [9].

longitudinal resistivity increase in magnitude. While the step-like, QQHE kink in  $\rho_{xy}$  is visible for each sample, the character of  $\rho_{xx}$  changes significantly as a function of  $n$ . In Sample D (Fig. 3d), the clear lump in  $\rho_{xx}$  at  $\sim 5.7$  T coincides with the reduced slope in  $\rho_{xy}$ , indicative of a QQHE contribution. Clearly, the size of the QQHE signal in Fig. 3d is large compared to the non-QQHE background. To demonstrate the relative contributions of the QQHE and the background magnetoresistance, we plot the QQHE contribution,  $\alpha H \partial_H \rho_{xy}$ , as light colored traces for  $\mu_0 H > 0$  T in Fig. 3a-d. The overall proportionality constant,  $\alpha$ , is chosen to match the size of the lump-like feature in  $\rho_{xx}$ . For Sample D, this simple

scaling works incredibly well. With decreasing  $n$ , this scaling progressively worsens: while the correlations of the features in  $\rho_{xx}$  and  $\rho_{xy}$  originating from the QQHE hold, an additional background component grows serving to obfuscate the  $\rho_{xx}$  QQHE features.

We hypothesize that this non-QQHE  $\rho_{xx}$  background and its apparent dependence on the carrier density originates from Coulomb disorder. At high carrier densities, Cd $_3$ As $_2$  is in the weak Coulomb disorder limit,  $eV_0 < E_F$ , accompanied by linear MR (Samples D, E). As the carrier density (and requisitely  $E_F$ ) shrink, the magnitude of the average disorder potential increases because of reduced screening. Shrinking  $E_F$  and increasing  $eV_0$  moves

the system from weak to strong Coulomb disorder, with  $eV_0 > E_F$ . Recently, the effects of strong Coulomb disorder on the magnetoresistance of TSMs has been theoretically predicted [29]. The magnetoresistance was shown to be a variable function of field, ranging from quadratic to linear, contingent upon the strength of the disorder and the magnitude of the applied magnetic field. After Ref. [29], the strong Coulomb disorder magnetoresistance is expected to behave as  $\sim H^2$  in the low field limit. With increasing field, the dependence crosses over to  $\sim H \log \delta \sqrt{H}$ . We construct a simple empirical model to describe our longitudinal resistivity that combines the QQHE resistivity scaling with the expected magnetoresistance in the limit of strong Coulomb disorder:

$$\rho_{xx} - \rho_0 = \alpha H \partial_H \rho_{xy} + f(H, H_c, w) \beta H^2 + f(H, H_c, -w) \gamma H \log \delta \sqrt{H}, \quad (1)$$

where  $\rho_0$  is the zero field resistivity,  $\alpha$  scales the QQHE, and  $\beta$  and  $\gamma$  are fitting parameters that scale the quadratic and sub-quadratic strong Coulomb disorder magnetoresistivities respectively, and  $\delta$  is a fitting parameter related to the disorder strength and the Fermi velocity.  $f(H, H_c, w) = (\exp((H - H_c)/w) + 1)^{-1}$  is a simple Fermi function that serves to smoothly crossover between different regimes of the strong Coulomb disorder magnetoresistivity. We fix  $H_c = 9.6$  T and  $w = 1.5$  T, serving as global values for all samples. The fitting is only performed for Samples A-C as the strong Coulomb disorder magnetoresistance breaks down with increasing carrier density. In Supplementary Note 2, we discuss the regimes of validity of this empirical expression.

Fits of Equation 1 to  $\rho_{xx}$  are shown as gray lines in Fig. 3a-c, demonstrating good agreement for all samples. Fig. 3i shows  $\beta$  and  $\gamma$  as a function of carrier density (a table of all fitting parameters can be found in Supplementary Note 3). We find similar values of  $\delta \sim 0.32$  T $^{-1/2}$  for Samples A-C. The QQHE scaling factor lies between  $\alpha \sim 0.17 - 0.35$  for all samples. Consistent with our expectations from the raw  $\rho_{xx}(H)$ ,  $\beta$  and  $\gamma$  decrease with increasing  $n$  as the disorder becomes weaker with increased screening. At the same time, the QQHE component comprises a larger portion of the measured  $\rho_{xx}$ . This is consistent with a crossover from strong-to-weak Coulomb disorder with increasing carrier density. In the weak Coulomb disorder limit (Sample D), the magnetoresistance scales linearly with field and the 2D QHE scaling relation,  $H \partial_H \rho_{xy}$ , captures the QQHE and the effects of weak Coulomb disorder simultaneously. We highlight that while the 2D QHE resistivity scaling relation seems to hold in Cd<sub>3</sub>As<sub>2</sub>, it may differ in other QQHE systems.

Cd<sub>3</sub>As<sub>2</sub> occupies a unique space in the search for 3D QQHE materials. Systems with small carrier densities are the route to observe QQHE and MBE affords us this tunability in Cd<sub>3</sub>As<sub>2</sub>. At the same time, shrinking  $E_F$  increases the effects of Coulomb disorder in Cd<sub>3</sub>As<sub>2</sub>:

the average disorder potential increases, charge puddling smears the Fermi level throughout, Landau levels are broadened, and importantly scattering from the screened Coulomb disorder changes character as  $eV_0/E_F$  grows. Fig. 3j summarizes this effect, showing that Cd<sub>3</sub>As<sub>2</sub> crosses into a regime of strong Coulomb disorder with decreasing Fermi level. As we have hypothesized and shown, the contribution from the Coulomb disorder scattering grows relative to the QQHE contribution with decreasing carrier density. Cumulatively, the effects of larger  $eV_0$  with decreasing  $E_F$  conspire to partially obstruct the QQHE in Cd<sub>3</sub>As<sub>2</sub>. A balance must be reached: while low  $n$  enables the observation of QQHE in Cd<sub>3</sub>As<sub>2</sub> in the first place, it simultaneously reduces screening of charged defects, which in turn obscures the QQHE.

## DISCUSSION

Though some reports on thin film Cd<sub>3</sub>As<sub>2</sub> have observed similar magnetotransport to that shown here [30–32], our results represent the first study of its kind to understand the experimental low carrier density magnetotransport as an amalgamation of a 3D QQHE and Coulomb disorder. In fact, it is Coulomb disorder that rules the roost of magnetotransport as the Fermi level is brought close to the Dirac point. Our study positions Cd<sub>3</sub>As<sub>2</sub> as a platform for exploring the 3D QQHE in a *gapless* Dirac system in the presence of tunable disorder. Our description intuitively extrapolates from the theoretically and experimentally motivated presence of significant Coulomb disorder in Dirac systems like Cd<sub>3</sub>As<sub>2</sub> and Na<sub>3</sub>Bi [9, 17, 19, 21, 22]. The recent development of the 3D QQHE has brought an understanding that quasi-quantized  $\rho_{xy}$  and the corresponding  $\rho_{xx}$  lumps (an extension of quantum oscillations) are the rule – not the exception – in low carrier density systems [7, 8]. We anticipate increasing the film mobilities and minimizing the effects of Coulomb disorder are avenues for enhancing the QQHE in Cd<sub>3</sub>As<sub>2</sub>.

It is instructive to consider our framework in the context of the pentatelluride systems. Plateaus and peaks much sharper than those presented here have been observed in ZrTe<sub>5</sub> [7, 10]. Where is the Coulomb disorder background in this case? First, a larger dielectric constant in ZrTe<sub>5</sub> [24] helps to more effectively screen charged point defects and reduce  $eV_0$ . Additionally, different growth conditions in ZrTe<sub>5</sub> can alter the observed Coulomb disorder. A recent STM study on chemical vapor transport (CVT) and flux grown crystals revealed significant charge puddling only in CVT-grown samples, which tend to have more Te vacancies resulting in more charged defects [33]. Most literature reports on QQHE or 3D QHE in ZrTe<sub>5</sub> are obtained on flux-grown crystals. The signatures of QQHE in CVT grown crystals are slightly obscured as compared to their flux grown

counterparts, likely indicative of higher charged defect concentrations (and corequisitely larger carrier densities) [23–25]. Our study implies that this difference in part stems from differences in Coulomb disorder in these crystals. As a result of lower defect charged point defect concentrations and greater screening, we estimate a disorder potential of a few meV in the pentatelluride systems as shown in Fig. 3j.

Broadly speaking, efforts to study 3D QHE in TSMs and low density metals will confront the realities of Coulomb disorder. We anticipate the QQHE to be more easily observable in systems with less prevalent charged disorder. We highlight that strategies that only reduce the Fermi level in TSMs will be met with the knock-on effects of reduced screening of charged defects: stronger Coulomb disorder scattering and broadening of LBs. Charged disorder must be simultaneously and independently addressed. Unlike bulk, thin film semimetals like those presented here offer tunability to realistically control and manipulate charge disorder. Passivation of charged point defects may be a promising route towards enhancing 3D QHE. In the case of  $\text{Cd}_3\text{As}_2$ , gating experiments in bulk-like films will allow direct tuning of the Coulomb disorder strength in single samples, helping to understand these mechanisms. In part, the realization of a 3D QHE phase with vanishing  $\rho_{xx}$  as well as the more exotic fractionalized analogue awaits an understanding of how to manipulate and tune this disorder.

## SUMMARY

In summary, we have observed evidence of the 3D QQHE in low carrier density, (001)-oriented  $\text{Cd}_3\text{As}_2$  thin films. Our picture identifies Coulomb disorder as the common thread linking evolving magnetotransport behavior across the spectrum of varying carrier density and  $E_F$  in  $\text{Cd}_3\text{As}_2$ , helping to unite a broad swath of observed magnetotransport reported in the literature. In reducing the carrier density in our films, we have probed the effects of the transition from weak-to-strong Coulomb disorder. With decreasing carrier density, the strength of Coulomb disorder increases, leading to the observation of strong Coulomb disorder magnetoresistivity in concert with the 3D QQHE. Coulomb disorder is centrally influential in TSMs and serves to conflate clear QL transport in  $\text{Cd}_3\text{As}_2$ . This work will be undoubtedly useful in the burgeoning studies exploring QQHE in low density metals and semimetals as well as the ongoing efforts to understand the effects of disorder as topological semimetals transition from fundamental curiosities to application.

## ACKNOWLEDGEMENTS

This work was authored in part by the National Renewable Energy Laboratory, operated by Alliance for Sustainable Energy, LLC, for the U.S. Department of Energy (DOE) under Contract No. DE-AC36-08GO28308.

Funding was provided by the U.S. Department of Energy, Office of Science, Basic Energy Sciences, Division of Materials Sciences and Engineering, Physical Behavior of Materials Program under the Disorder in Topological Semimetals project.

The work at Sandia is supported by the LDRD program.

The views expressed in the article do not necessarily represent the views of the DOE or the U.S. Government. The U.S. Government retains and the publisher, by accepting the article for publication, acknowledges that the U.S. Government retains a nonexclusive, paid-up, irrevocable, worldwide license to publish or reproduce the published form of this work, or allow others to do so, for U.S. Government purposes.

We would like to thank Igor Žutić, Konstantin Denisov, and Rebecca Smaha for useful discussions.

## METHODS

**Film Growth** Films were grown as described elsewhere on GaAs(001) substrates [34].  $\text{Cd}_3\text{As}_2$  layers were grown from separate Cd and As effusion sources on lattice matched  $\text{Zn}_x\text{Te}_{1-x}$  buffers using As rich conditions at 115 C. All samples have bulk-like thicknesses, ranging from 200-560 nm.

**Electrical Transport**  $\text{Cd}_3\text{As}_2$  Hall bars with 6 electroplated Au contacts were fabricated using standard wet photolithography. Electrical transport measurements were performed using a Keithley 2182 Nanovoltmeter and 6221A DC current source in a Quantum Design Physical Property Measurement System. Carrier densities are extracted from the low field ( $\mu_0 H < 1$  T slopes of  $\rho_{xy}$ ).

**Theoretical Model** We model the electronic structure of bulk  $\text{Cd}_3\text{As}_2$  by using a k.p approach based on 4 orbitals ( $s, p_{x,y,z}$ ) and two spins [35]. The corresponding Hamiltonian also contains a spin-orbit coupling term [35] as well a Zeeman term. The Hamiltonian (of size  $8 \times 8$ ) is a function of three parameters, i.e. the 3 k-space vectors  $k_x, k_y, k_z$ .

In order to take into account the Landau bands (LB) created by the application of an external magnetic field (chosen to align with the  $z$ -direction), we apply the so-called Peierls transformation and quantize the parameters  $k_x, k_y$  in the plane perpendicular to the field into non-commuting operators [36, 37]. The latter are themselves expressed in term of creation and annihilation operators ( $a^\dagger$  and  $a$ ) of the harmonic-oscillator-like states associated with the Landau bands (now labeled by the

integer number  $n_{\text{LB}}$  [38–40]. Upon the transformation  $H(k_x, k_y, k_z) \rightarrow H(a, a^\dagger; k_z)$ , the new Hamiltonian is parameterized by only one wave-vector, i.e.  $k_z$  parallel to the direction of the applied field. The new Hamiltonian has now a size of  $(8 \times (n_{\text{LB}}^{\text{max}} + 1))^2$  where  $n_{\text{LB}}^{\text{max}}$  corresponds to the maximum number of LBs used in the calculations.

The Hamiltonian is diagonalized for each value of the parameter  $k_z$  to give the eigenvalues  $E_{m, n_{\text{LB}}}(k_z)$  and eigenstates  $|\Psi_{m, n_{\text{LB}}}(k_z)\rangle$ , where  $m$  labels the original  $sp$  plus spin orbitals,  $n_{\text{LB}}$  labels the different LB and  $k_z$  is the only left continuous parameter. From these eigenstates and from the velocity matrices  $\nabla_{k_\alpha} H(k_x, k_y, k_z)$  (transformed into the LB basis), we can calculate the conductivity  $\sigma_{\alpha\beta}$  ( $\alpha, \beta = x, y, z$ ) within linear response theory [41–43]. The Hall conductivity  $\sigma_{xy}$  is obtained from the Berry curvature of the states as described in [44]. For all our calculations of the electronic structure and the conductivities, we have carefully checked the convergence of the result versus the maximum number of LB  $n_{\text{LB}}^{\text{max}}$  used. The longitudinal resistivity is calculated from the standard expression  $\rho_{xx} = \sigma_{xx}/(\sigma_{xx}^2 + \sigma_{xy}^2)$ . Note that from the symmetry of the Hamiltonian and a magnetic field applied in the  $z$ -direction, one has  $\sigma_{xx} = \sigma_{yy}$  and  $\sigma_{xy} = -\sigma_{yx}$ . In the disorder-free case, we always find  $\sigma_{xy} \gg \sigma_{xx}$ , hence  $\rho_{xx} \sim \sigma_{xx}/\sigma_{xy}^2$  and  $\rho_{xy} = \sigma_{xy}/(\sigma_{xx}^2 + \sigma_{xy}^2) \sim 1/\sigma_{xy}$ .

Disorder-free calculations produce, as expected, the "rounded" plateaux in the Hall conductivity versus applied field which is characteristic of the 3D quasi-QHE, accompanied with peak-like structure in the longitudinal conductivity (as shown in Figure 1b and in Supplementary Note 1) located at the onset of the plateaux in the Hall conductivity. All these features correspond to magnetic field values for which a LB crosses the Fermi level of the Dirac/Weyl semimetal. For more information on the inclusion of disorder, please see Supplementary Note 1.

## AUTHOR CONTRIBUTIONS

All authors contributed to the preparation of the manuscript. K. A., I. L., J. N., and A. R. conceived and designed experiments. I. L., J. N., and A. R. performed the experiments. I. L. and H. N. analyzed the data. I. L., J. N., H. N., A. R., and M. v. S. contributed materials or analysis tools.

## SUPPLEMENTAL INFORMATION

The supplement gives more detailed information about 1) the theoretical k.p model and the inclusion of disorder in theoretical calculations of the magnetotransport, 2) the strong Coulomb disorder model, and 3) the strong Coulomb disorder fitting parameters.

## DATA AVAILABILITY

The data that support the findings of this study are available from the corresponding author upon reasonable request.

---

\* *Current Affiliation: First Solar Inc., 1035 Walsh Ave., Santa Clara, 95050, CA, United States*

† *Kirstin.Alberi@nrel.gov*

- [1] K. V. Klitzing, G. Dorda, and M. Pepper, New Method for High-Accuracy Determination of the Fine-Structure Constant Based on Quantized Hall Resistance, *Physical Review Letters* **45**, 494 (1980).
- [2] K. Von Klitzing, The quantized Hall effect, *Reviews of Modern Physics* **58**, 519 (1986).
- [3] R. B. Laughlin, Quantized Hall conductivity in two dimensions, *Physical Review B* **23**, 5632 (1981).
- [4] B. I. Halperin, Quantized Hall conductance, current-carrying edge states, and the existence of extended states in a two-dimensional disordered potential, *Physical Review B* **25**, 2185 (1982).
- [5] W. Yu, W. Pan, D. Medlin, M. Rodriguez, S. Lee, Z.-q. Bao, and F. Zhang,  $\pi$  and  $4\pi$  Josephson effects mediated by a Dirac semimetal, *Physical Review Letters* **120**, 177704 (2018).
- [6] P. Li, W. Wu, Y. Wen, C. Zhang, J. Zhang, S. Zhang, Z. Yu, S. A. Yang, A. Manchon, and X.-x. Zhang, Spin-momentum locking and spin-orbit torques in magnetic nano-heterojunctions composed of Weyl semimetal WTe<sub>2</sub>, *Nature Communications* **9**, 3990 (2018).
- [7] F. Tang, Y. Ren, P. Wang, R. Zhong, J. Schneeloch, S. A. Yang, K. Yang, P. A. Lee, G. Gu, Z. Qiao, and L. Zhang, Three-dimensional quantum Hall effect and metal-insulator transition in ZrTe<sub>5</sub>, *Nature* **569**, 537 (2019).
- [8] J. Gooth, S. Galeski, and T. Meng, Quantum-Hall physics and three dimensions, *Reports on Progress in Physics* **86**, 044501 (2023).
- [9] B. Skinner, Coulomb disorder in three-dimensional Dirac systems, *Physical Review B* **90**, 060202 (2014).
- [10] S. Galeski, T. Ehmcke, R. Wawrzyńczak, P. M. Lozano, K. Cho, A. Sharma, S. Das, F. Küster, P. Sessi, M. Brando, R. Kuchler, A. Markou, M. König, P. Swekis, C. Felser, Y. Sassa, Q. Li, G. Gu, M. V. Zimmermann, O. Ivashko, D. I. Gorbunov, S. Zherlitsyn, T. Förster, S. S. P. Parkin, J. Wosnitza, T. Meng, and J. Gooth, Origin of the quasi-quantized Hall effect in ZrTe<sub>5</sub>, *Nature Communications* **12**, 3197 (2021).
- [11] N. R. Cooper and J. T. Chalker, Coulomb interactions and the integer quantum Hall effect: Screening and transport, *Physical Review B* **48**, 4530 (1993).
- [12] H. L. Stormer, Nobel Lecture: The fractional quantum Hall effect, *Reviews of Modern Physics* **71**, 875 (1999).
- [13] K. Manna, N. Kumar, S. Chattopadhyay, J. Noky, M. Yao, J. Park, T. Förster, M. Uhlarz, T. Chakraborty, B. V. Schwarze, J. Hornung, V. N. Strocov, H. Borrmann, C. Shekhar, Y. Sun, J. Wosnitza, C. Felser, and J. Gooth, Three-dimensional quasi-quantized Hall insulator phase in Sr Si<sub>2</sub>, *Physical Review B* **106**, L041113 (2022).



- [14] R. Wawrzyńczak, S. Galeski, J. Noky, Y. Sun, C. Felser, and J. Gooth, Quasi-quantized Hall response in bulk InAs, *Scientific Reports* **12**, 2153 (2022).
- [15] S. Galeski, X. Zhao, R. Wawrzyńczak, T. Meng, T. Förster, P. M. Lozano, S. Honnali, N. Lamba, T. Ehmcke, A. Markou, Q. Li., G. Gu, W. Zhu, J. Wosnitza, C. Felser, G. F. Chen, and J. Gooth, Unconventional Hall response in the quantum limit of HfTe<sub>5</sub>, *Nature Communications* **11**, 5926 (2020).
- [16] M. M. Piva, R. Wawrzyńczak, N. Kumar, L. O. Kutelak, G. A. Lombardi, R. D. Dos Reis, C. Felser, and M. Nicklas, Importance of the semimetallic state for the quantum Hall effect in HfTe<sub>5</sub>, *Physical Review Materials* **8**, L041202 (2024).
- [17] J. C. W. Song, G. Refael, and P. A. Lee, Linear magnetoresistance in metals: Guiding center diffusion in a smooth random potential, *Physical Review B* **92**, 180204 (2015).
- [18] C. Brooks, M. Van Schilfgaarde, D. Pashov, J. N. Nelson, K. Alberi, D. S. Dessau, and S. Lany, Band energy dependence of defect formation in the topological semimetal Cd<sub>3</sub>As<sub>2</sub>, *Physical Review B* **107**, 224110 (2023).
- [19] J. N. Nelson, I. A. Leahy, A. D. Rice, C. Brooks, G. Teeter, M. Van Schilfgaarde, S. Lany, B. Fluegel, M. Lee, and K. Alberi, Direct link between disorder and magnetoresistance in topological semimetals, *Physical Review B* **107**, L220206 (2023).
- [20] S. Jeon, B. B. Zhou, A. Gyenis, B. E. Feldman, I. Kimchi, A. C. Potter, Q. D. Gibson, R. J. Cava, A. Vishwanath, and A. Yazdani, Landau quantization and quasiparticle interference in the three-dimensional Dirac semimetal Cd<sub>3</sub>As<sub>2</sub>, *Nature Materials* **13**, 851 (2014).
- [21] M. T. Edmonds, J. L. Collins, J. Hellerstedt, I. Yudhistrira, L. C. Gomes, J. N. B. Rodrigues, S. Adam, and M. S. Fuhrer, Spatial charge inhomogeneity and defect states in topological Dirac semimetal thin films of Na<sub>3</sub>Bi, *Science Advances* **3**, eaa06661 (2017).
- [22] I. A. Leahy, Y.-P. Lin, P. E. Siegfried, A. C. Treglia, J. C. W. Song, R. M. Nandkishore, and M. Lee, Non-saturating large magnetoresistance in semimetals, *Proceedings of the National Academy of Sciences* **115**, 10570 (2018).
- [23] W. Wang, X. Zhang, H. Xu, Y. Zhao, W. Zou, L. He, and Y. Xu, Evidence for Layered Quantized Transport in Dirac Semimetal ZrTe<sub>5</sub>, *Scientific Reports* **8**, 5125 (2018).
- [24] A. Gourgout, M. Leroux, J.-L. Smirr, M. Massoudzadegan, R. P. S. M. Lobo, D. Vignolles, C. Proust, H. Berger, Q. Li, G. Gu, C. C. Homes, A. Akrap, and B. Fauqué, Magnetic freeze-out and anomalous Hall effect in ZrTe<sub>5</sub>, *npj Quantum Materials* **7**, 71 (2022).
- [25] P. Shahi, D. Singh, J. Sun, L. Zhao, G. Chen, Y. Lv, J. Li, J.-Q. Yan, D. Mandrus, and J.-G. Cheng, Bipolar Conduction as the Possible Origin of the Electronic Transition in Pentatellurides: Metallic vs Semiconducting Behavior, *Physical Review X* **8**, 021055 (2018).
- [26] B. Zhao, P. Cheng, H. Pan, S. Zhang, B. Wang, G. Wang, F. Xiu, and F. Song, Weak antilocalization in Cd<sub>3</sub>As<sub>2</sub> thin films, *Scientific Reports* **6**, 22377 (2016).
- [27] W. Yu, D. X. Rademacher, N. R. Valdez, M. A. Rodriguez, T. M. Nenoff, and W. Pan, Evidence of decoupling of surface and bulk states in Dirac semimetal cd<sub>3</sub>as<sub>2</sub>, *Nanotechnology* **33**, 415002 (2022).
- [28] I. A. Leahy, A. D. Rice, C.-S. Jiang, G. Paul, K. Alberi, and J. N. Nelson, Anisotropic weak antilocalization in thin films of the Weyl semimetal TaAs, *Physical Review B* **110**, 054206 (2024).
- [29] Y. I. Rodionov, K. I. Kugel, and B. A. Aronson, Quantum magnetoresistance of weyl semimetals with strong coulomb disorder, *Phys. Rev. B* **107**, 155120 (2023).
- [30] C. Zhang, A. Narayan, S. Lu, J. Zhang, H. Zhang, Z. Ni, X. Yuan, Y. Liu, J.-H. Park, E. Zhang, W. Wang, S. Liu, L. Cheng, L. Pi, Z. Sheng, S. Sanvito, and F. Xiu, Evolution of Weyl orbit and quantum Hall effect in Dirac semimetal Cd<sub>3</sub>As<sub>2</sub>, *Nature Communications* **8**, 1272 (2017).
- [31] C. Zhang, Y. Zhang, X. Yuan, S. Lu, J. Zhang, A. Narayan, Y. Liu, H. Zhang, Z. Ni, R. Liu, E. S. Choi, A. Suslov, S. Sanvito, L. Pi, H.-Z. Lu, A. C. Potter, and F. Xiu, Quantum Hall effect based on Weyl orbits in Cd<sub>3</sub>As<sub>2</sub>, *Nature* **565**, 331 (2019).
- [32] Y. Nakazawa, M. Uchida, S. Nishihaya, S. Sato, A. Nakao, J. Matsuno, and M. Kawasaki, Molecular beam epitaxy of three-dimensionally thick Dirac semimetal Cd<sub>3</sub>As<sub>2</sub> films, *APL Materials* **7**, 071109 (2019).
- [33] B. Salzmann, A. Pulkkinen, B. Hildebrand, T. Jaouen, S. N. Zhang, E. Martino, Q. Li, G. Gu, H. Berger, O. V. Yazyev, A. Akrap, and C. Monney, Nature of native atomic defects in ZrTe<sub>5</sub> and their impact on the low-energy electronic structure, *Physical Review Materials* **4**, 114201 (2020).
- [34] A. D. Rice, C. H. Lee, B. Fluegel, A. G. Norman, J. N. Nelson, C. S. Jiang, M. Steger, D. L. McGott, P. Walker, and K. Alberi, Epitaxial Dirac Semimetal Vertical Heterostructures for Advanced Device Architectures, *Advanced Functional Materials* **32**, 2111470 (2022).
- [35] Z. Wang, H. Weng, Q. Wu, X. Dai, and Z. Fang, Three-dimensional dirac semimetal and quantum transport in cd<sub>3</sub>as<sub>2</sub>, *Phys. Rev. B* **88**, 125427 (2013).
- [36] J. M. Luttinger and W. Kohn, Motion of electrons and holes in perturbed periodic fields, *Phys. Rev.* **97**, 869 (1955).
- [37] P. G. Harper, Magnetic gauge transformations in solid-state problems, *Journal of Physics: Condensed Matter* **3**, 3047 (1991).
- [38] S. Jeon, B. B. Zhou, A. Gyenis, B. E. Feldman, I. Kimchi, A. C. Potter, Q. D. Gibson, R. J. Cava, A. Vishwanath, and A. Yazdani, Landau quantization and quasiparticle interference in the three-dimensional dirac semimetal cd<sub>3</sub>as<sub>2</sub>, *Nature Materials* **13**, 851 (2014).
- [39] W. Miao, B. Guo, S. Stemmer, and X. Dai, Engineering the in-plane anomalous hall effect in cd<sub>3</sub>as<sub>2</sub> thin films, *Phys. Rev. B* **109**, 155408.
- [40] M. Smith, V. L. Quito, A. A. Burkov, P. P. Orth, and I. Martin, Theory for cd<sub>3</sub>as<sub>2</sub> thin films in the presence of magnetic fields, *Phys. Rev. B* **109**, 155136 (2024).
- [41] A. Bastin, C. Lewiner, O. Betbeder-Matibet, and P. Nozieres, Quantum oscillations of the Hall effect of a Fermion gas with random impurity scattering, *J. Phys. Chem. Solids* **32**, 1811 (1971).
- [42] A. Crépieux and P. Bruno, Theory of the anomalous hall effect from the kubo formula and the dirac equation, *Phys. Rev. B* **64**, 014416 (2001).
- [43] T. Morimoto and H. Aoki, Flow diagram of the longitudinal and hall conductivities in ac regime in the disordered graphene quantum hall system, *Journal of Physics: Conference Series* **400**, 042047 (2012).

- [44] M. Gradhand, D. V. Fedorov, F. Pientka, P. Zahn, I. Mertig, and B. L. Györfy, First-principle calculations of the berry curvature of bloch states for charge and spin transport of electrons, *Journal of Physics: Condensed Matter* **24**, 213202 (2012).